JOURNAL OF MATERIALS SCIENCE 30 (1995) 3487–3500

Two-dimensional SiC–C–SiC(O)$_{fibre}$ composite

Part I *Microstructural evolution at high temperature in different atmospheres*

M. BACKHAUS-RICOULT, N. MOZDZIERZ
Centres d'Etudes de Chimie et Metallurgie, CNRS, 15 Rue G. Urbain. 94407 Vitry, France

Under thermodynamically well defined conditions, "reducing", "neutral" and "oxidizing" atmospheres, a two-dimensional SiC–C–SiC(O)$_{fibre}$ composite was annealed at different temperatures and times. The microstructural evolution has been studied from a macroscopical scale down to the atomic level by scanning election microscopy (SEM), transmission electron microscopy (TEM), energy dispersive spectroscopy (EDX), (EELS) and HREM. Corrosion models have been developed; in all atmospheres the corrosion scale grows from the surface into the bulk, giving rise to a very irregular scale due to coarse macroporosity. At high temperature, the fibre degrades by decomposition of its oxycarbide phase and by Ostwald ripening of the silicon carbide and graphite crystals inside the fibre. In oxidizing and neutral atmospheres a silica surface scale forms. In oxidizing and neutral atmospheres, the carbon interphase is gradually substituted by a silica layer or mixed silica/silicon carbide layer, respectively, with increasing thickness. In reducing atmosphere, the degradation is the most important since no protective layer forms around the fibre. The carbon interphase reacts with the oxycarbide of the fibre and forms gaseous products and silicon carbide, which replaces the carbon interphase.

1. Introduction

The development of ceramic matrix composites (CMC) has gone through a spectacular evolution over the last twenty years, especially for applications in automotive, aeronautic and aerospace engineering. CMCs were originally developed for high temperature applications in liquid propulsion, motors and aircraft engines. The first generations of CMCs, the C/C composites, were mechanically reliable at high temperatures, but were too sensitive to oxidation. Therefore, further development efforts were geared towards carbon-free composites. The first step was a substitution of the carbon matrix by silicon carbide. Then, the carbon fibres were substituted by silicon carbide-containing fibres. Two types of fibres were then mainly used. The first type comprises a central carbon filament of large diameter surrounded by a silicon carbide coating (Avco or Textron fibre) [1–4]. Interphase layers of varying nature (different deposition conditions and compositions) are deposited on top of the silicon carbide, yielding thereby mixtures of carbon and SiC of various morphologies. The second family of fibres is obtained by pyrolysis of organic precursors and includes Nicalon fibre and new generations of amorphous Si–C–O or Si–C–N fibres. For the latter ones the polysilanes were molten and spun, before being decomposed at higher temperatures to form amorphous or microcrystalline fibres, depending on the decomposition conditions [4–8].

The mechanical properties of pure "SiC" fibre–SiC matrix composites are not satisfactory, because of the strong interface between matrix and fibre. For this reason, an additional weak interphase was added to the composite. The most common approach is the addition of a carbon interphase, in the case of Nicalon fibres, or of a mixed carbon/silicon carbide interphase with optimized morphology in the case of the AVCO fibre. New developments have resulted in the substitution of the easily oxidizable carbon interphase by either a metal layer (molybdenum, for instance), a thin boron nitride or boron carbide layer, or a mixed silicon carbide/carbon layer [9–11].

In the present work, we examine the microstructural evolution of a two-dimensional SiC (Nicalon fibre)/C/SiC composite as a function of different annealing atmospheres and temperatures. Three thermodynamically well defined atmospheres were chosen, which correspond to oxidizing, neutral and reducing environment around the composite. Detailed microscopy observations of the reaction scales were performed down to the atomic scale and coupled to chemical analysis. Based on these observations, the materials microstructure could be well understood and the material degradation modelled in terms of thermodynamics and kinetics.

2. Experimental procedure

2.1. Materials

The 2-D SiC–C–SiC composite used for this investigation was provided in the form of 2-mm thick plates. It consists of a two-dimensional network of Nicalon

0022–2461

fibre (NLM 202) bundles, which are coated by chemical vapour infiltration with a carbon layer. The SiC matrix is deposited afterwards in subsequent cycles, by chemical vapour infiltration. The final density of the material is 2.5–2.6 $g\,cm^{-3}$. It contains about 10% porosity, which can be divided in an intertoronal porosity, characterized by a large pore size (0.3–0.5 mm) and in an intratoronal porosity, with small pore size (2–10 μm). The total fibre content is 40 vol %.

2.2. Annealing conditions

Samples of dimensions 4 mm × 2 mm × 2 mm were cut from the SiC–C–SiC plate and polished with diamond paste (final grit size: 2 μm). These parallelepipeds were then annealed at temperatures ranging from 1123 K to 1673 K, a range through which the degradation of Nicalon fibre can be followed. Three types of atmospheres, reducing, neutral and oxidizing, were used for the annealing experiments. To set thermodynamically well defined annealing conditions for the ternary composite system studied (for each annealing condition, the activities of all components were fixed at the sample surface), not only the oxygen activity, but another component activity also had to be fixed at the material surface. This other component activity was determined by placing the sample surface in direct contact with an appropriate pure solid phase: SiC/C for reducing conditions or SiO_2/SiC for neutral and oxidizing conditions. Annealing times were varied from 1 to 100 h in order to follow the kinetics for each condition.

2.2.1. Annealing in "reducing" atmosphere

Polished samples were placed in a graphite die and embedded in SiC powder, in order to fix the activities of carbon and silicon carbide to 1. The thermal treatments were made in a furnace with graphite heating elements, operated under a static argon atmosphere at 1×10^5 Pa. The residual oxygen content is then given by traces of air present in the vacuum and by the impurity content in the argon gas as 0.27 Pa. At high temperature, residual oxygen reacts almost entirely with carbon of the furnace to form CO. The final oxygen activity at reaction temperature is therefore determined by the C/CO buffer (for example, 2×10^{-27} at 1673 K and 3×10^{-30} at 1423 K). Oxygen outgassing from the samples during reduction results in an increase of the oxygen partial pressure in the static atmosphere (for example, up to 6×10^{-17} Pa after 100 h at 1673 K).

2.2.2. Annealing in "neutral" atmosphere

Polished samples were placed on a SiC platelet, inside a closed alumina tube furnace and annealed in an argon flow of 10 $l\,h^{-1}$ with residual oxygen partial pressure of 0.7 Pa. Since in such conditions silicon carbide is oxidized, as in the oxidizing case the activity of silica is one, while the oxygen activity is set by the level of residual oxygen in the gas.

2.2.3. Annealing in "oxidizing" atmosphere

Polished samples were placed on silicon carbide platelets or in silica tubes, inside an alumina tube furnace and annealed in an air flow of 10 $l\,h^{-1}$. In these conditions, the oxygen activity is fixed as 0.21 in the gas and the silica activity is fixed as 1 (set by contact between the oxidized SiC platelet and the oxidation scale of the sample itself, the oxidation of both materials yielding immediate formation of a pure SiO_2 surface layer).

2.3. Sample observation

The starting material and the differently annealed samples were investigated by optical microscopy, scanning electron microscopy (SEM), electron microprobe analysis and transmission electron microscopy (TEM). Optical microscopy observation was used to evaluate pore size distribution and homogeneity of fibre distribution.

Outer surfaces and polished cross-sections of the starting material and of the differently annealed samples were observed by SEM. A Jeol JSM 840 operated at 20 keV was used for secondary and backscattered imaging. A Philips 501B, equipped with an energy dispersive detector, with particularly good resolution for light elements, was used for qualitative and quantitative chemical analysis (7 keV). Quantification was done by direct comparison of the sample with adequate elemental standards (graphite or SiC for carbon; SiO_2, Al_2O_3 or MgO for oxygen, silicon, silica or silicon carbide for silicon). Part of quantitative analyses was also made with a Cameca microprobe at 10 kV with standards: SiC for carbon, $Y_3Fe_5O_{12}$ for oxygen and SiC or SiO_2 for silicon.

TEM samples were prepared by carefully cutting slices of 300 μm thickness from annealed and non-annealed materials, polishing them down to a thickness of 40–50 μm, with 8 μm diamond paste and ion-milling them in a cold stage by argon bombardment at 5 kV, until perforation. All types of embedding materials or infiltrated epoxy were avoided, to prevent both from polluting the composite interfaces with an amorphous (polymeric) phase and from the risk of generating cracks in the material, as a result of thermal mismatch with the epoxy.

TEM observations were made with a Jeol 2000FX operated at 200 keV and equipped with a thin-window energy dispersive X-ray detector and a PEELS detector. For quantitative analysis, a cooled beryllium sample holder was available. This equipment allowed chemical and structural analysis of regions as small as 5 nm. High resolution imaging of the composite was made in part with the Jeol 2000FX (point to point resolution 0.28 nm) and with an Akachi 002B (point to point resolution 0.18 nm).

3. Experimental results

3.1. As-received composite

The Nicalon fibres constituting the composite are assembled in torons made of about 500 filaments and interwoven into a two-dimensional network (see Fig. 1). The longitudinal torons are observed to be

either in phase or out of phase, thereby producing an irregular architecture with a distribution of large pores. The fibre diameter varies from 10 to 26 μm. In the as-received material the fibres present homogeneous contrast in secondary and backscattered imaging (SEM), as shown in Fig. 2(a). Multiple analyses inside a fibre or of different fibres yield reproducible chemical composition, depending only on the nature of the standard used. The different results are shown in Table I.

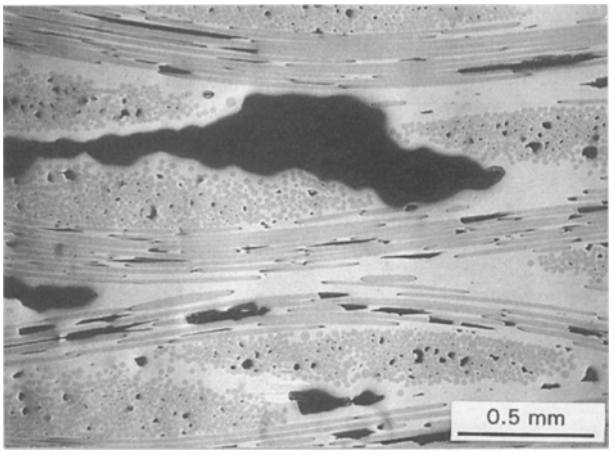

Figure 1 Optical micrograph showing the geometrical structure of the SiC–C–SiC composite.

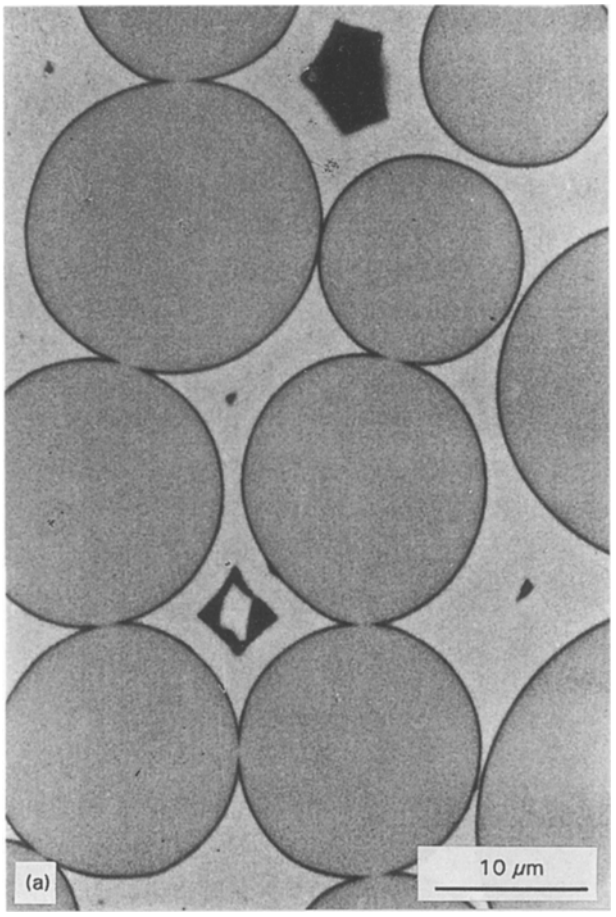

Figure 2 As-received composite. (a) Scanning electron micrograph showing the fibre with the carbon interphase embedded in the SiC matrix; (b) TEM micrograph of the interface region between fibre, carbon layer and SiC matrix; (c) HREM image and corresponding electron diffraction patterns of the fibre, indicating the carbon and silicon carbide crystals inside the fibre.

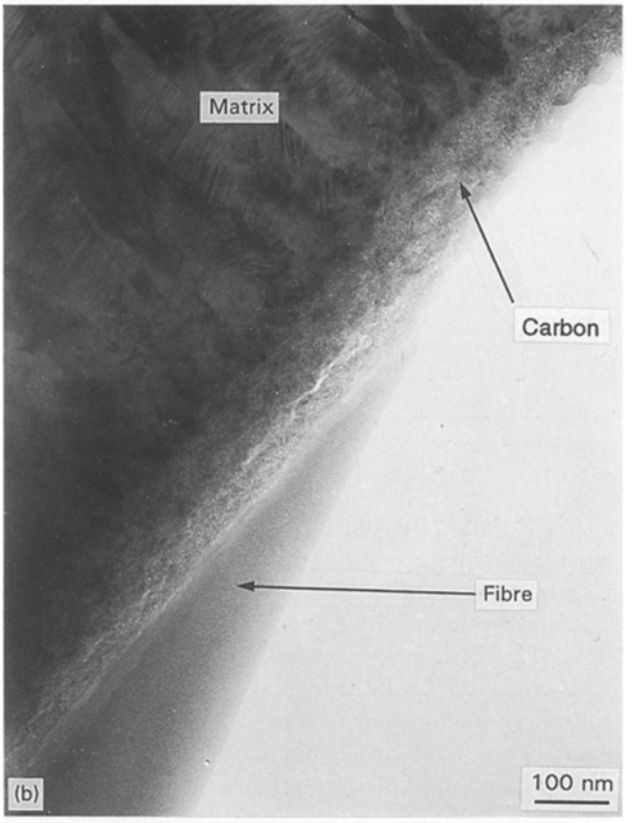

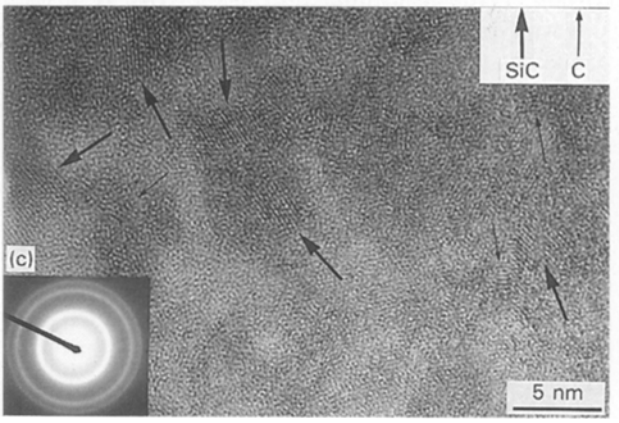

Figure 2 (contd.).

SEM imaging reveals the presence of a thin carbon layer around the fibres (Fig. 2(a)). Under certain conditions of accelerating voltage and electron beam current, it is possible to separate the consecutive infiltration layers composing the silicon carbide CVI matrix. They are spread in irregular circles around the fibres.

TEM observations (Fig. 2(b)) allow a more detailed view of the composite: Broadening and splitting of the continuous rings observed in the electron diffraction pattern of the fibre is the evidence that this fibre is multiphase and nanocrystalline, with average crystal size of 2–3 nm. The different phases present in the fibre can be separated by high resolution imaging (Fig. 2(c)): they are silicon carbide crystals and carbon crystals surrounded by an amorphous phase. The SiC crystals have an average size of 3 nm. Their measured lattice parameters, 0.25 nm and 0.21 nm, were identified

TABLE I Chemical analysis of the fibre in the starting material obtained by SEM, Microprobe or TEM using different standards

	Standards	C (wt %)	Si (wt %)	O (wt %)
SEM	C for C, Si for Si, SiO_2 for O	47	42	11
	SiC for C, Si for Si, SiO_2 for O	28	57	15
	SiC for C, SiC for Si, SiO_2 for O	28	58	14
	SiC for C, SiC for Si, Al_2O_3 for O	28	58	14
	SiC for C, SiC for Si, MgO for O	28	59	13
MP	SiC for C, SiC for Si, $Y_3Fe_5O_{12}$ for O	29	58	13
	SiC for C, SiO_2 for Si, $Y_3Fe_5O_{12}$ for O	31	56	13
TEM	SiC for C, SiC for Si, SiO_2 for O			
	near the interface fibre/carbon	32	53	15
	core of fibre	30	57	13

précision $\pm$ 1 wt %.

as {1 1 1} and {2 0 0} planes of the β-SiC structure. The crystals are regularly distributed all over the fibre. Lattice planes can only be resolved in those crystals oriented along the [0 1 1] zone axis and tilted by less than 10°. This represents about 5% of the total crystals, which can be extrapolated to a total amount of silicon carbide crystals on the order of 50–60 vol %.

Carbon crystals inside the fibre are smaller, 1 nm and less, and present an interplanar spacing, 0.35 nm, typical of graphite. A total volume fraction of 20–30% carbon crystals is estimated from the HREM images.

Both types of crystals, β-SiC and graphite, are embedded in an amorphous phase, which contains all three elements, carbon, oxygen and silicon. The chemical composition of this silicon oxycarbide phase was determined in two ways: From high resolution images, the fibre is seen to contain 20–30 vol % carbon, 50–60 vol % silicon carbide and a complement of 10–30 vol % amorphous phase. Based on this estimate and on global chemical analysis of the fibre (made by SEM/EDX on bulk samples and TEM/EDX on thin sections; see Table I), the composition of the oxycarbide phase can be deduced: $SiO_{1.52}C_{0.6-1.05}$. Local information on chemical composition and type of chemical bonding in the oxycarbide phase are obtained by combining EELS and EDX with high spatial resolution, as detailed in Part II of this work [12]. The absorption edge measured for silicon (101 eV) shows that this element is present in the amorphous phase with a bonding type intermediate between that of SiC (absorption edge at 99 eV) and that of SiO_2 (absorption edge at 104 eV). The finite structure of the silicon edge can be simulated by overlaying silicon carbide spectra and a silica spectrum in the ratio 1:0.35. The value and structure of the oxygen absorption edge are unchanged compared to pure silica, which indicates that oxygen bonding is the same in silicon oxycarbide and in silica. The carbon absorption edge has the typical structure of silicon carbide, with a small contribution of the fine structure of pure carbon, as a consequence of the mixed bonding character of carbon, as free carbon and as silicon carbide.

The thickness of the carbon interphase surrounding the fibres present in the as-received composite can be measured by TEM, see Fig. 2(b); it is homogeneous around a single fibre, but varies from fibre to fibre. Electron diffraction of the carbon interphase (see Fig. 2(b)) consists of two half-moon intensity regions, characteristic of either turbostratic or microporous carbon. The orientation of the diffracted half-moons varies across the interphase, indicating structural changes, which can be confirmed by HREM imaging and PEELS spectroscopy of the interphase region (as shown in Part II of this work [12]). Next to the fibre interface, the basal planes of carbon are oriented parallel to the interface over a thickness of 2–5 nm (graphite-like carbon). At the centre of the interphase, carbon becomes less organized and forms typical turbostratic carbon units, 4 nm × 4 nm × 6 nm blocks, with varying orientation of their basal plane. On the matrix side of the interphase (a 20 nm layer), the carbon retrieves its graphitic character. The basal plane is preferentially parallel to the interface, forming parallel layers or cauliflower-like structures. The different bonding states adopted by carbon at various locations of the interphase are confirmed by the evolution of the fine structure of the carbon absorption edge in EELS spectra. In particular, a peak broadening is observed for increasing deviations from the perfect graphite structure.

The silicon carbide CVI matrix mainly consists of β-SiC. The interphase is in direct contact with an infiltration layer. The contact zone consists of small (about 50 nm) equiaxial grains intimately contacting each other, see Fig. 2(b). The following zone is made of columnar grains having a typical diameter of 160–300 nm. The c-axes of these grains are almost parallel, as a result of CVI growth. Stacking fault density in these grains is high. Second and third CVI cycles are characterized by columns of larger dimensions than the first ones. A thin amorphous layer is visible between the individual infiltration cycles. These amorphous layers are connected to the columnar scale by small equiaxial grains. They are very fragile and constitute zones of preferential crack propagation under thermal or mechanical stresses.

3.2. Composite annealed under reducing atmosphere

At temperatures below 1423 K, the composite degrades slowly, see Fig. 3. Only after about 100 h at 1123 K or 25 h at 1423 K small gas bubbles start to

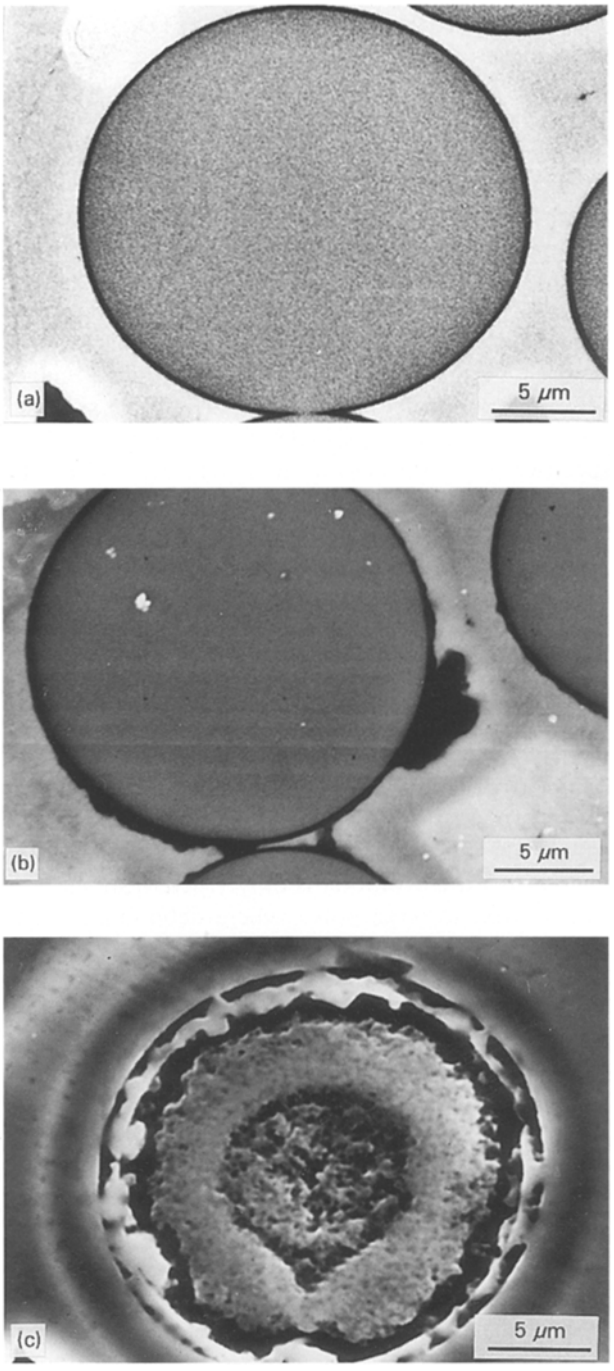

Figure 3 SEM micrographs showing the microstructural evolution of the composite, near the surface after annealing in reducing atmosphere. (a) 1123 K, 100 h; (b) 1423 K, 100 h; (c) 1673 K, 50 h.

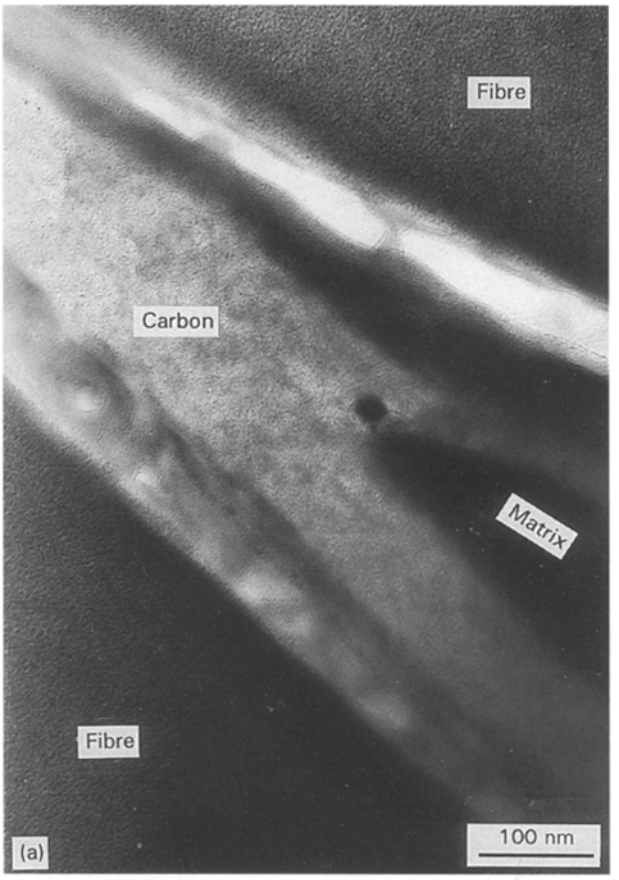

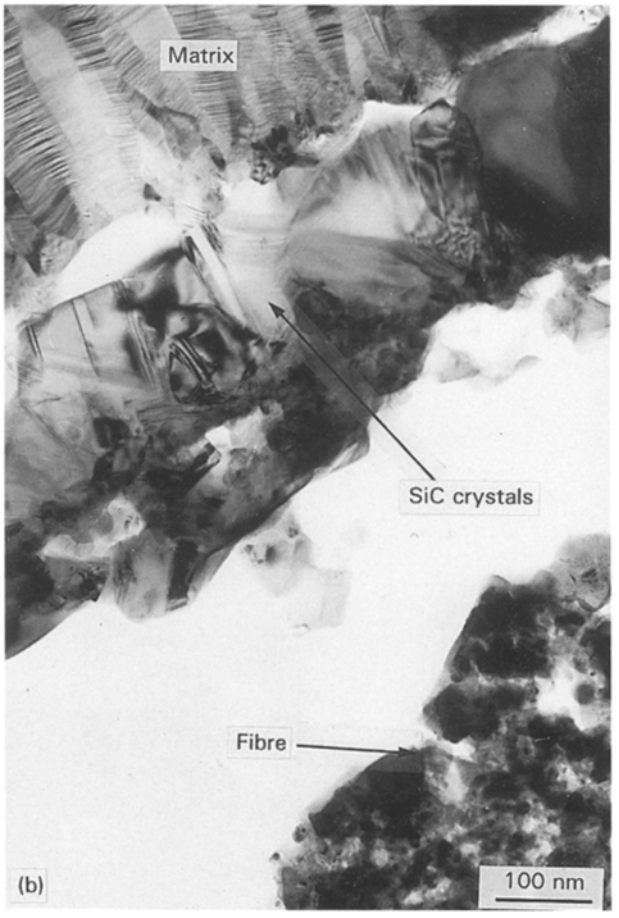

Figure 4 TEM micrographs of the composite annealed in reducing atmosphere, (a) showing pore formation inside the carbon interphase at 1613 K after 50 h: (b) showing the formation of a pore channel which is partially filled by SiC crystals at 1673 K after 50 h.

form inside the carbon interphase. For longer annealing times, for example 50 and 100 h at 1423 K, the carbon interphase begins to be consumed, starting at the sample outer surface, and yielding a gap around the fibres next to the surface.

At higher temperature, 1613 K, the reaction becomes more important and propagates more rapidly into the bulk; TEM observation of a sample annealed during 50 h shows that, even in the bulk, the carbon interphase has lost its continuity, upon small pore formation (gas bubbles) or debonding of the interface between fibre and carbon interphase (Fig. 4(a)).

At 1673 K, the carbon interphase is rapidly consumed. The reaction migrates from the surface into the bulk. TEM observation of samples annealed for 4 and

10 h shows that the bulk material remains unmodified. For longer annealing times (> 25 h) (see Fig. 3) the carbon interphase is consumed over the whole sample: decohesion of the interfaces and formation of a large gap between fibre and matrix can be seen in the TEM (Fig. 4(b)). This gap can be filled by small silicon carbide crystals. Size and density of the silicon carbide crystals increase with annealing time. After 10 days, a dense silicon carbide ring completely fills the gap around the fibre. The average size of the crystals is 0.2–0.5 μm after 25 h, 0.5–2 μm after 50 h. These newly-formed silicon carbide crystals are almost always in contact with the matrix, rarely with the fibre. They do not show the columnar growth of the matrix and are less faulted than the matrix grains.

Up to 1423 K, fibres in the bulk material basically keep their initial structure, recrystallization remaining minor. At 1613 K, recrystallization of the fibre develops, yielding a non-homogeneous honeycomb-like contrast of the fibres in SEM. TEM dark-field imaging, HREM imaging and electron diffraction patterns show the corresponding increase in size of the silicon carbide crystals in the fibre (Fig. 5). In the electron diffraction pattern, the intensity rings are broader and split into characteristic SiC and C rings. After 50 h at 1653 K, silicon carbide crystals have grown to 5–10 nm, while only a small size increase is noticed for carbon crystals (up to 5 nm). After an anneal of 50 h at 1653 K, 90–95% of the fibres are recrystallized.

With increasing temperature fibre recrystallization accelerates and propagates. At 1673 K, fibres next to macropores or to the surface become porous within a few hours. Pores of diameter up to 0.1 μm after 4 h and 1 μm after 10 h can be observed. EDX analysis of fibres close to the outer surface indicates a significant oxygen loss: 63 wt % Si, 31 wt % C and 5 wt % O. The phase distribution in the fibres has become very inhomogeneous. After 50 h, this depletion increases and oxygen concentrations as low as 2–4% are detected in fibres close to the surface. In the bulk material, the fibre composition remains unchanged. Electron diffraction of the transformed fibres shows small discrete spots, evidence of extended recrystallization of the fibres. Indeed, a silicon carbide crystal size of 30–70 nm could be measured from dark-field images of samples annealed for 50 h. For the same samples, the small peak characteristic of silica in the PEELS spectra has disappeared in the fine structure. HREM imaging reveals a variation in crystal size over the fibre: near the fibre surface the crystals are on average smaller than in the central region. The larger crystals are faceted and faulted in the basal plane. They are frequently grown together leaving not more than two to three atomic planes of amorphous film present at their connections.

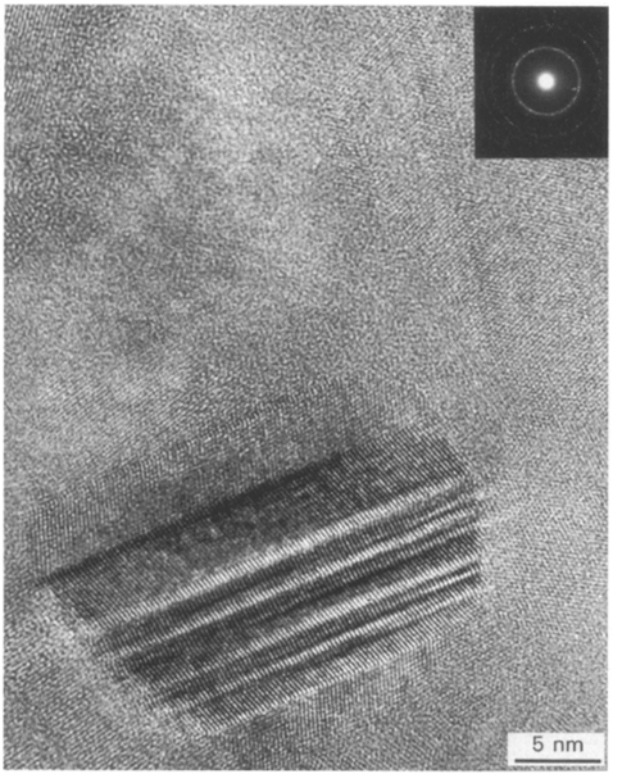

Figure 5 HREM image and corresponding electron diffraction pattern of the fibre after annealing in reducing atmosphere at 1673 K for 50 h.

3.3. Composite annealed in neutral atmosphere

After annealing the composite at 1123 K for 100 h, microstructural evolution is only visible near the surface or next to large pores, where debonding of the interface between interphase and matrix occurs. In the bulk material, the carbon layer is preserved. At temperatures above 1373 K, a silica scale forms on the sample surfaces. This scale grows with annealing time and temperature. In its first stage, it is inhomogeneous and contains featherlike nuclei which become progressively interconnected with time. The silica layer is at the origin of large stresses at its interface, yielding important debonding of the fibre–matrix interfaces close to the surface.

In the bulk material, the interphase is already degraded after 50 h of annealing (Fig. 6). The carbon ring around the fibres has become inhomogeneous. For longer annealing times it is substituted by a double layer characterized by two different chemical contrasts (SEM backscattered imaging). Close to the sample surface this layer is no longer subdivided, but contains either many small pores or a continuous crack in its central part. SEM–EDX analyses reveal that this layer is always silica.

No change (within 1%) in the global chemistry of the fibre can be determined at 1423 K, even for long annealing times. At high temperatures (1673 K) TEM investigations reveal an important recrystallization of the fibre and a high degree of porosity. After 25 and 50 h, the size of the silicon carbide crystals in the fibre is 10–20 nm and 20–40 nm, respectively. The crystals are faceted and faulted on the basal plane.

At 1673 K the carbon interphase deteriorates faster than at 1423 K, but again the same steps are observed for the substitution of the carbon interphase (Fig. 6). Initially, small pores and cracks form inside the carbon layer, then the carbon coating around the fibres becomes discontinuous and partly disappears. It is

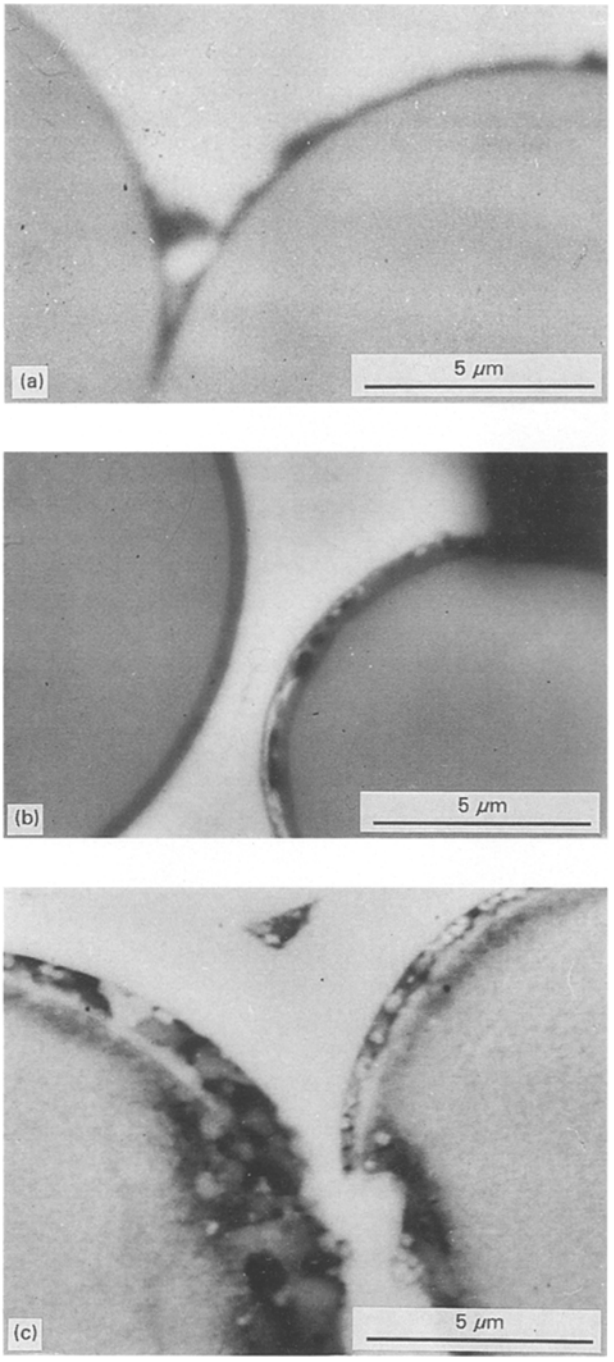

Figure 6 SEM micrographs showing microstructural evolution of the composite, near the surface after annealing in neutral atmosphere. (a) 1123 K, 100 h; (b) 1423 K, 50 h; (c) 1673 K, 50 h.

substituted by a silica layer, evidenced by double contrast in SEM backscattered electron images. This difference in chemical contrast could be related by TEM to the complex structure of the oxidation scale (Fig. 7). EDX and EELS analyses show that carbon has completely disappeared in the "interphase" after 50 h. It is replaced by a layer of amorphous silica, which reaches a thickness of 120 nm and 150–300 nm after 25 and 50 h, respectively. This layer contains large silicon carbide crystals, up to 100 or 200 nm in size. These crystals grow preferentially on the fibre side of the silica layer and are then at the origin of the double contrast observed by SEM. After 25 h of annealing, carbon residues are still observed by TEM at the matrix side in contact with the silica layer.

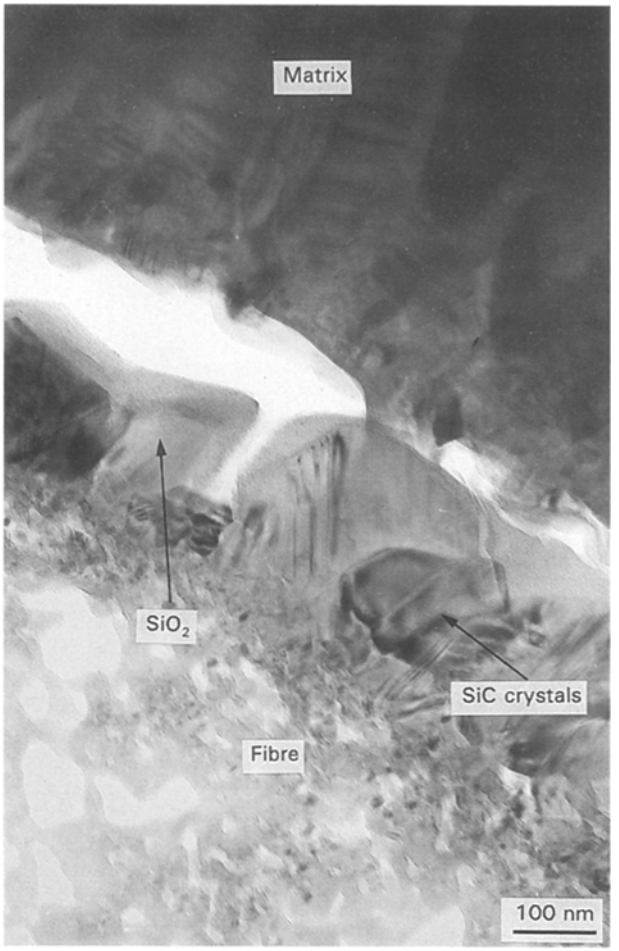

Figure 7 TEM micrograph of the composite interphase after anneal in neutral atmosphere (1673 K, 50 h), showing formation of a mixed silica, silicon carbide layer replacing the carbon interphase.

3.4. Composite annealed in oxidizing atmosphere

In oxidizing atmosphere a thin silica layer covers the entire composite surface. For temperatures as low as 1123 K, the thickness of this film remains negligible and is only visible through its optical reflections. However, it protects the composite against further oxidation, yielding even after 100 h in air at 1123 K a corrosion depth of only 10 μm in which the carbon interphase has become discontinuous. Voids and small cracks have preferentially formed at the interface between fibre and carbon layer (see Fig. 8).

At 1673 K, the reaction is more important: After 1 or 4 h in air, SEM imaging contrast of the carbon interphase around the fibres next to the surface is inhomogeneous, showing two separated half rings. EDX analysis shows that at one side of the fibre the carbon interface is preserved while a silica layer has already formed at the other side. In these conditions, the silica layer has a thickness between 0.3 and 0.6 μm. After 25 h, the composite is more strongly affected by oxidation. In the regions close to the sample surface, the carbon interphase is substituted by an amorphous silica layer, as seen from electron diffraction [12]. SEM investigations show that the silica layer thickness varies from 0.5–0.8 μm close to the sample surface to only 0.1–0.2 μm in the bulk, where the carbon

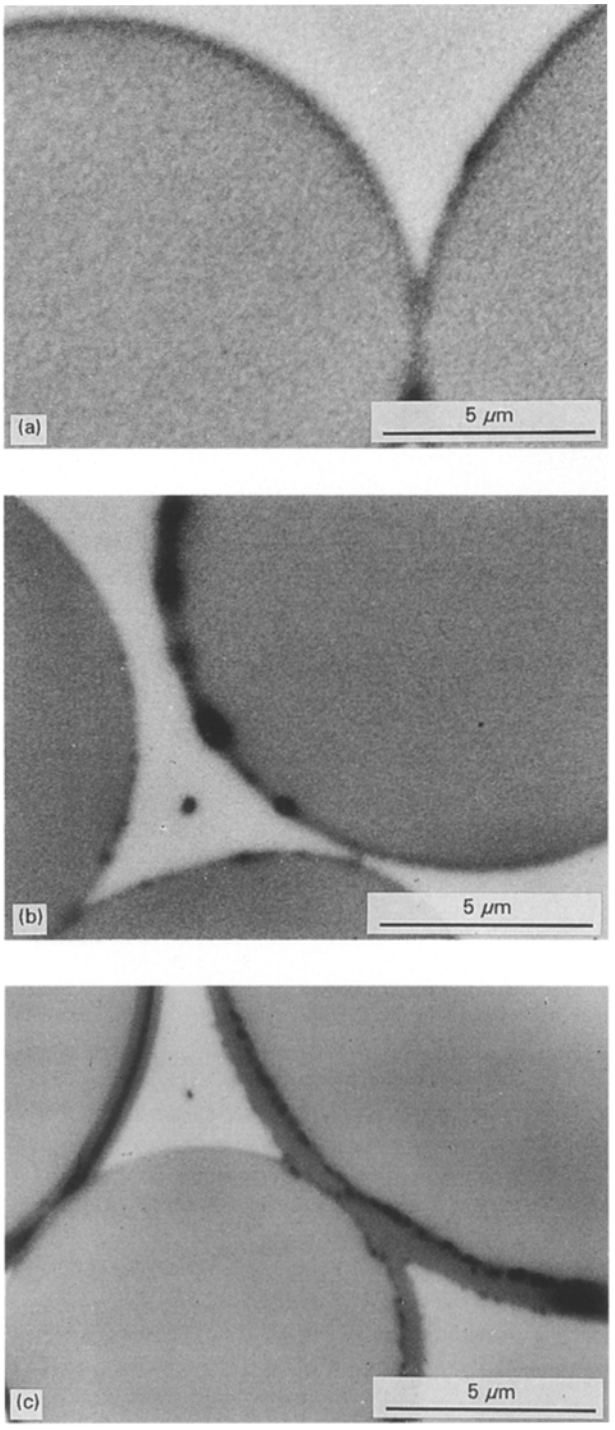

Figure 8 SEM micrographs of the composite annealed in oxidizing atmosphere indicating the different oxidation steps of the carbon interphase. (a) 1123 K, 100 h, air; (b) 1423 K, 50 h, air; (c) 1673 K, 10 h, oxygen activity 10^{-3}.

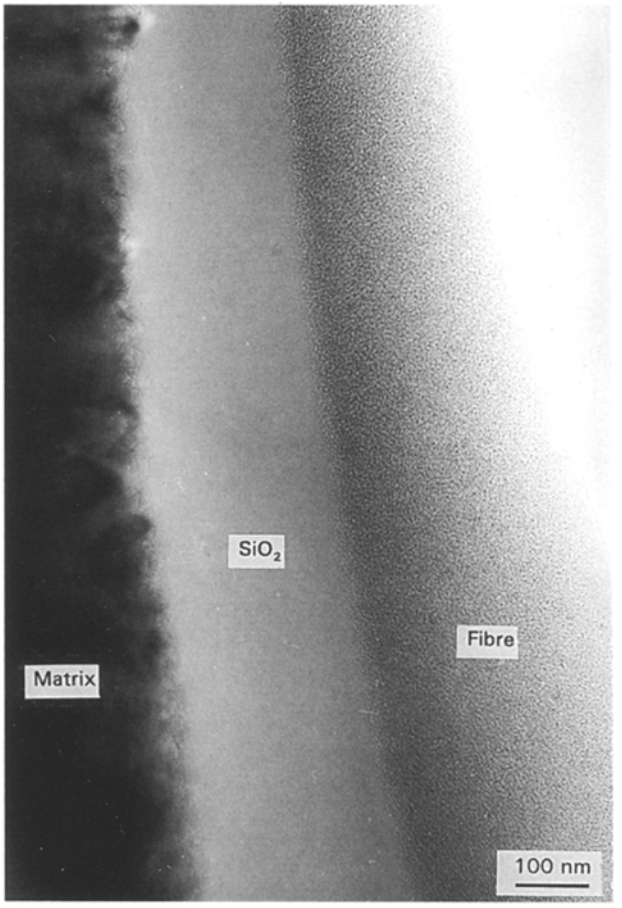

Figure 9 TEM micrograph of the interfacial region between matrix and fibre with the amorphous silica layer which formed by oxidation at 1673 K for 25 h.

interphase is still preserved. The observation of fibre cross-sections (Fig. 8) from bulk to sample surface shows the different oxidation steps. Local oxidation starts with the formation of small voids or gas bubbles in the carbon interphase, which agglomerate to finally develop into a continuous crack between the fibre and the matrix. The carbon layer is progressively substituted blockwise (these blocks are circular segments) by silica; a double layer of silica and carbon on top of each other has never been observed. After complete substitution of the carbon interphase, the silica layer thickness increases. In its core, the layer contains small gas bubbles and, closer to the other surface, a continuous crack could even be observed. With increasing annealing time the silica layers surrounding the fibres become thicker and some of the larger porosities in the composite are filled with silica. After 50 h at $a_{O_2} = 10^{-3}$ silica layers of 1–1.5 μm are observed around the fibres in regions close to the surface. The interface between the shrinking fibre and the silica product layer is not smooth on a microscopic scale. In the TEM, it is even difficult to distinguish the silica layer from the fibre, because in their outer regions the fibres contain much less crystals and more amorphous silica or silicon oxycarbide.

For all different oxidizing conditions the silica layer has proved to be amorphous (see Fig. 9). No recrystallization was detected by electron diffraction and high resolution imaging, at the temperatures studied [12].

SEM imaging of fibres close to the surface does not reveal any contrast change, proving that the fibres remain homogeneous. EDX analysis indicates a global oxygen content increase in the fibres next to the surface, yielding compositions about 60 wt % Si, 24 wt % C and 16 wt % O at 1673 K. In the bulk, the composition of the starting material is preserved. TEM studies show that the level of fibre recrystallization effectively remains minor. Even after 25 h at 1673 K, the silicon carbide crystal size does not exceed 5–10 nm. At oxygen partial pressures lower than that of air, but still oxidizing, $a_{O_2} = 10^{-3}$, the oxidation

mechanism is identical to that observed in air, though with a slower oxidation rate. The microstructural evolution could then be followed in more detail.

4. Discussion

4.1. Composite thermodynamical stability at high temperature

The SiC/C/Nicalon-fibre composite is made of multiple phases of the three elements silicon, carbon and oxygen. Therefore, it must be described as a multiphase ternary system. The coexistence of two phases of the Si–C–O system implies that all component activities in both phases are fixed and forbids thermodynamical equilibrium coexistence with other phases of the system.

Our TEM observations of the composite have shown that the fibre consists of 50–60 vol % SiC crystals of size averaging 3 nm and of 20–30 vol % graphite crystals of size on the order of 1 nm, which are embedded inside an amorphous silicon oxycarbide matrix of average composition $SiO_{1.52}C_{0.6-1.05}$ [13–19]. The fibres are surrounded by an interphase layer of turbostratic carbon and by the SiC matrix [20–23]. The simple thermodynamic statement made above is enough to indicate that the SiC/C/fibre composite is a metastable material whose existence relies only on sluggish kinetics.

During high temperature annealing the sluggish kinetics are overpowered and the system evolves towards its equilibrium state. Most of the amorphous metastable silicon oxycarbide decomposes into silicon carbide, silica and carbon, as experimentally observed for heat-treated Nicalon fibres [24–29], [17], [19] and for black glasses of similar compositions [30–31]. Ostwald ripening of the multiphase fibre occurs, resulting in the coarsening of silicon carbide and graphite crystals of the fibre and thereby in a decrease of the interfacial energy term of the Gibbs energy. Such a coarsening of the crystals present in the fibre was specially observed at the high temperatures (1673 K) investigated here, where the crystal size increases by a factor of ten after 25 h. At 1423 K and lower temperatures, Ostwald ripening remains negligible and does not much affect the fibre structure. High resolution imaging has brought the evidence of an increase of the crystalline fraction of the fibre, which must be accounted for by decomposition of the amorphous oxycarbide phase.

Since equilibrium coexistence of the three final decomposition products of the fibre (silica, silicon carbide and carbon) is thermodynamically impossible, these products react. Thermodynamic calculations have shown that the fibre material decomposes at high temperature under formation of CO (CO_2 at lower temperature) and SiO (SiO_2 at lower temperature). Considering in first approximation that the composite material (as well as the fibres present in its bulk) is a closed system, the implication is that the fibre inside the composite readily decomposes under the simple effect of high temperature into SiO and CO, according to the following reactions:

$$3C + \underline{SiO_2} \Rightarrow SiC + 2CO$$

$$\Delta G^R = +39\ \text{kJ mol}^{-1}(1673\ \text{K}) \quad (1)$$

$$SiC + \underline{SiO_2} \Rightarrow 2SiO + C$$

$$\Delta G^R = +190\ \text{kJ mol}^{-1}(1673\ \text{K}) \quad (2)$$

($\underline{SiO_2}$ stands for silica in solution in the oxycarbide phase.)

The gaseous products, CO and SiO, evolved during this decomposition rapidly build-up very large partial pressures in the closed system. When the partial pressure reaches equillibrium activities, chemical degradation stops.

At the interface between fibre and carbon interphase layer, fibre decomposition can occur by reaction with carbon of the interphase (ip), but again restricted by the formation of entrapped gaseous products:

$$3C(ip) + \underline{SiO_2} \Rightarrow SiC + 2CO \quad (3)$$

$$C(f) \Rightarrow C(ip) \quad (4)$$

Only in the case of an open system, such as fibres in contact with the outer surface or with macropores, is fibre degradation not limited by the formation of gaseous products, since no pressure builds up. For CO and SiO (in surrounding atmosphere) partial pressures not corresponding to the equilibrium values of the fibre, fibres next to the surface decompose continuously as described above. This is supported by our microscopy observations. Only minor changes of the bulk material are observed for short annealing times. Fibres have undergone Ostwald ripening, silicon oxycarbide has partly decomposed, but no gas or pore formation is observed after low temperature annealing. These observations indicate that, at low temperatures, fibres can be considered as the above described closed system. At higher temperatures, such as 1673 K, and especially in a reducing atmosphere, where no protective layer is formed around the fibre, the fibre must be considered as an open system; it decomposes rapidly. A high degree of porosity (gas bubbles) is seen in the fibre by TEM, after exposure to a reducing atmosphere.

Fibre degradation in an open system is observed at the sample surface. Especially in the case of reducing atmosphere, a porous surface layer containing gas bubbles forms on top of the fibres. In oxidizing or neutral atmosphere, the formation of feather-like silica nuclei or continuous silica layers is observed on the fibres.

4.2. Analysis of the annealing conditions

From a fundamental point of view it is well known that in ternary systems two component activities must be fixed to thermodynamically determine the system. This fact is well known for oxide and silicate systems, but it is often neglected in studies about composite corrosion. The annealing conditions of our experiments with the ternary Si–C–O system were selected in such a way that two component activities (the third

one being consequently also fixed) were fixed at the sample surface.

In a reducing environment silicon carbide and carbon activities are fixed to unity by contact of the composite surface with the two solid phases. CO partial pressure (and consequently oxygen partial pressure) is fixed by residual oxygen to 5×10^{-6} (increasing to 3×10^{-3} upon reduction) at 1673 K (see Table II).

In an oxidizing environment the oxygen activity in the surrounding atmosphere was set by gas flow as $a_{O_2} = 0.21$ (air) or $a_{O_2} = 10^{-6}$ (neutral atmosphere). Silica activity was fixed to $a_{SiO_2} = 1$ by contact between the composite surface and the pure silica surface layer (oxidation product of the composite itself). The oxygen activity at the SiO_2/composite interface depends on the diffusion rate of oxygen through the scale, from the surface to the interface, on the diffusion rate of the gaseous product CO from the interface to the surface and on the chemical reaction rate itself. Even for the oxidation of pure SiC, these data are not exactly known [32] and therefore exact values for CO and O_2 activities at the interface cannot be given. If the chemical reaction is considered to be fast (local thermodynamic equilibrium is established at the interface) and very fast oxygen transport compared to slow carbon monoxide transport, then the outer oxygen activity of the gas is principally established at the interface. This would be expected to result in enormous CO partial pressures (about 10^{24}) and carbon formation at the contact with pure SiC. Since neither an intermediate carbon layer nor an explosion of the silica scale is observed, this limiting case can be ruled out. In the opposite case, rapid transport of CO and slow transport of oxygen across the scale are considered. As a result, silicon carbide at the interface becomes depleted in carbon. In extreme cases, the maximum nonstoichiometry of silicon carbide is reached, corresponding to a silicon activity of 1. The CO partial pressure at the interface is then $0.25 \leqslant a_{CO} \leqslant 1$. After Luthra [32] a mixed rate control actually occurs and it is therefore only possible to indicate limits for the oxygen partial pressure at the interface as indicated in Table II.

Component activities at the composite surface for the different annealing conditions and equilibrium activities of the composite phases are summarized in Tables II and III.

TABLE II Equilibrium activities of the different components in reducing, neutral and oxidizing atmosphere at 1423 and 1673 K

		1423 K	1673 K
reducing atmosphere	a_{O_2}	$3.3 \times 10^{-30} \rightarrow 9 \times 10^{-25}$	$2 \times 10^{-27} \rightarrow 6 \times 10^{-22}$
	a_{CO}	$5.4 \times 10^{-6} \rightarrow 2.8 \times 10^{-3}$	$5.4 \times 10^{-6} \rightarrow 2.8 \times 10^{-3}$
	a_C	1	1
	a_{SiC}	1	1
	a_{SiO}	$9.9 \times 10^{-9} \rightarrow 4.8 \times 10^{-6}$	$2.1 \times 10^{-8} \rightarrow 1.2 \times 10^{-5}$
	a_{SiO_2}	$7.9 \times 10^{-10} \rightarrow 2.2\,10^{-4}$	$4.10^{-10} \rightarrow 1.3\,10^{-4}$
neutral atmosphere	a_{O_2}	7×10^{-6}	7×10^{-6}
	a_{CO}	2.3×10^{24}[a]	4.6×10^{17}[a]
	a_C	$\gg 1$[a]	$\gg 1$[a]
	a_{SiC}	1	1
	a_{SiO}	7.8×10^{-12}	8.7×10^{-10}
	a_{SiO_2}	1	1
oxidizing atmosphere	a_{O_2}	0.21	0.21
			$10^{-20} \leqslant a_C \leqslant 10^{-17}$[b]
	a_{CO}	6.9×10^{28}[a]	2.4×10^{24}[a]
			$10^{-4} \leqslant a_C \leqslant 1$[b]
	a_C	$\gg 1$[a]	$\gg 1$[a]
			$0.013 \leqslant a_C \leqslant 1$[b]
	a_{SiC}	1	1
	a_{SiO}	4.5×10^{-14}	5×10^{-12}
	a_{SiO_2}	1	1

[a]with $a_{O_2} = a_{O_{2(g)}}$ at the interface SiO_2/composite
[b]Luthra [32].

4.3. Evolution of the composite in reducing atmosphere

Annealing in reducing atmosphere means that very low CO and SiO partial pressures are established at the composite surface (see Table II). The composite matrix is stable in contact with silicon carbide and carbon, but the fibres must decrease their CO and SiO activities to be in equilibrium with the conditions prevailing at the surface, resulting in their degradation, according to the above reactions (Equations 1–3). From Equation 1 silica in solution in the oxycarbide phase and graphite crystals in the fibre react to form CO gas and silicon carbide. From Equation 2 oxycarbide of the fibre can be decomposed by formation of gaseous SiO and silicon carbide. At the fibre surfaces the oxycarbide of the fibre can react according to Equation 3 in a similar way with carbon of the interphase. All three reactions imply a decrease of the oxygen content in the fibre, a decrease of the oxycarbide content and an increase of the silicon carbide content. This is exactly what we observed in the annealed samples. The reduction front propagates from the outer composite surface to the material bulk. The reduction kinetics cannot be determined in detail, due to the presence of extensive macroporosity, which constitutes fast short-circuit paths to the outer surface for gaseous components and also to the very complex two-dimensional microstructure of the composite, which yields an ill-defined spatial distribution of fast and slow diffusion and reaction paths. Therefore, our observations allow only a qualitative description of the kinetics. Attention should be paid to thermogravimetric measurements which yield a smooth

TABLE III Component activities in the different phases of the composite

	a_{O_2}	a_{CO}	a_C	a_{SiC}	a_{SiO}	a_{SiO_2}
fibre	$9 \times 10^{-21} \rightarrow 2 \times 10^{-20}$	$5 \times 10^{-2} \rightarrow 8 \times 10^{-2}$	4.66	3.3	$4 \times 10^{-5} \rightarrow 6 \times 10^{-5}$	$0.17 \rightarrow 0.36$
carbon (ip)			1			
matrix			1	1		

relationship between weight loss and annealing time. However, this type of measurement is only an average over the irregular and complex microstructure. On the contrary, our results provide insight about local microstructure and better show how the composite evolves on a micro- or nanoscale [33–36].

Thermodynamic considerations only tell that CO gas forms and that SiC grows as a solid phase. Chemical analysis on a microscale confirms that global fibre composition changes during reduction anneal, becoming depleted in oxygen. Nanoscale (TEM) observations finally tell where silicon carbide is formed, where gas evolves and how it is evacuated. During the reaction, the oxycarbide phase present in fibres loses part of its dissolved silica and gets richer in carbon and silicon carbide, and, in equilibrium with the crystallized phases of carbon and silicon carbide, exsolves carbon and silicon carbide. The amount and size of carbon crystals and also of silicon carbide crystals increase, as confirmed by HREM, leaving only thin oxycarbide grain boundary films which embed the crystals. During the reaction, the carbon monoxide activity increases to such a high level that many gas bubbles form within the fibre (observed by TEM). Bubble formation may be facilitated by the decrease of fibre volume. As depicted in Fig. 10, at the interface between fibre and carbon interphase, the reaction between silica dissolved in the oxycarbide phase and the carbon interphase (3) occurs again under formation of gaseous CO and consumption of the carbon layer. CO gas is evacuated along the interface or along the long open channels which form by carbon consumption. Again, the reaction results in a large volume decrease, in turn creating large stresses, which may cause formation of small pores inside the carbon interphase and extended decohesion of this interface (both observed by TEM). Silicon carbide, which grows by the reaction with the carbon interphase (3), forms on top of the silicon carbide matrix as crystals of size averaging 0.1 μm, which further grow with the on-going reaction. After consumption of the carbon interphase, these crystals continue to grow by reaction with the small carbon crystals present in the fibre next to the interphase and finally fill the pore channels around the fibre. The complete reaction scheme is depicted in Fig. 10.

4.4. Evolution of the composite in "neutral" atmosphere

As can be seen in Table II, "neutral atmosphere" corresponds to an oxidizing environment for the carbon interphase, the matrix and the fibre. Therefore, a microstructural evolution of the composite similar to the oxidizing case should be expected, but with more sluggish kinetics. This is only partly fulfilled. As in an oxidizing atmosphere, formation of a crystalline silica surface scale and consumption of the carbon interphase are observed. Contrary to the observations made for the oxidizing case, in a neutral atmosphere a mixed silica–silicon carbide layer may substitute the carbon interphase. This mixed scale appears only at high temperature and only next to the outer sample

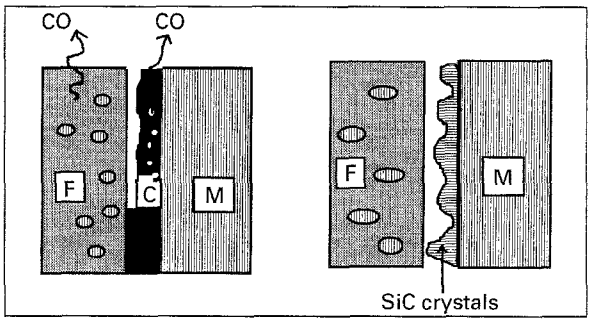

Figure 10 Reaction scheme for the degradation of the composite in reducing atmosphere (F-fibre, C-carbon, M-matrix).

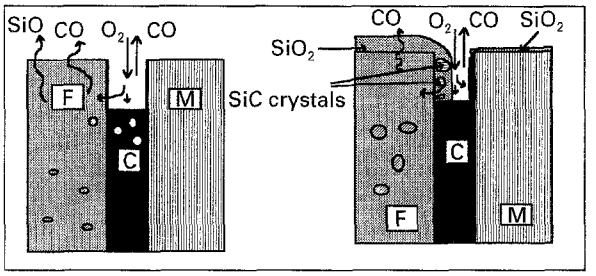

Figure 11 Reaction scheme for the degradation of the composite in neutral atmosphere.

surface and consists of amorphous silica with 0.1 μm large silicon carbide crystals on the fibre side. Deeper in the bulk or at lower temperatures, only silica was observed. This observation is in agreement with the report from Labrugère [33–34], who observed for similar conditions a mixed silica/carbon layer at low temperature and a mixed silica/silicon carbide layer at higher temperature.

The carbon interface is rapidly oxidised by the in-diffusing oxygen under formation of CO

$$C_{(ip)} + 1/2O_2 \rightarrow CO \qquad (5)$$

where oxygen penetrates through the so-formed pore channels around the fibres, while CO diffuses to the outer surface (Fig. 11).

The formation of the mixed silica–silicon carbide scale around the fibres in neutral atmosphere can be explained by equilibrium SiO activity dictated by the neutral atmosphere (Table II) which is much lower than that of the oxycarbide in the fibre (Table III). Consequently, the fibre decomposes not only under formation of the gaseous product CO as in air, but also by diminishing its SiO activity

$$SiO_xC_y + (1 + y - x)/2O_2 \rightarrow \text{“SiO”} + yCO \qquad (6)$$

The fibre becomes very porous upon the formation of the gaseous products, as confirmed by TEM observations. The gaseous products can diffuse through the porous reacted fibre and/or along open pore channels to the outer surface, where the "SiO" may further react.

At the interface between the fibre and carbon interphase, carbon of the interphase reacts with the excess SiO of the fibre, under formation of SiO_2 and SiC or CO

$$2\text{“SiO”} + C_{(ip)} \rightarrow SiO_2 + SiC \qquad (7)$$

$$\text{“SiO”} + 2C_{(ip)} \rightarrow SiC + CO \qquad (8)$$

yielding a mixed silica/silicon carbide layer on the fibre side, as shown in Fig. 11. Fibre and matrix next to the open pore channel are oxidized at a much slower rate than the carbon interphase, according to

$$SiC_{(m)} + 3/2O_2 \rightarrow SiO_2 + CO \quad (9)$$

$$SiC_{(f)} + 3/2O_2 \rightarrow SiO_2 + CO \quad (10)$$

$$C_{(f)} + 1/2O_2 \rightarrow CO \quad (11)$$

$$SiO_xC_{y(f)} + O_2 \rightarrow SiO_2 \text{ (or oxygen rich silicon oxycarbide)} + yCO \quad (12)$$

Then a thin silica layer forms on top of the matrix side of the pore channel, while on the fibre side after the reaction with the carbon layer further oxidation occurs by forming a growing silica layer on top of the mixed silica/silicon carbide layer. Since the oxidation is very slow, even after long reaction times the pore channels are not filled. This model is supported by our observations for high temperatures.

Further away from the surface (due to the activity gradient across the pore channel) or at lower temperatures, the SiO activity is closer to the equilibrium values of the silicon oxycarbide of the fibre. As in the oxidizing case, the oxidation of the oxycarbide inside the fibre results in formation of silica as the only oxidation product (see Equation 12), yielding a simple silica oxidation scale on the fibre side.

The formation on a metastable silicon oxycarbide layer as oxidation product of the fibres, which decomposes for longer annealing times into silica and silicon carbide is ruled out as an explanation because of the relatively large size of the silicon carbide crystals and their irregular distribution in the layer.

4.5. Evolution of the composite in oxidizing atmosphere

At the temperature and oxygen partial pressure investigated in this report, silica and carbon monoxide are the only products of the oxidation of the composite. Taking into account the microstructure of the composite, several oxidation steps can be considered, as depicted in Fig. 12. Carbon interphases intersecting the outer surface are easily oxidized, leaving pore channels which interconnect the remaining carbon interphase in the bulk material with the outer surface. Carbon monoxide escapes through the pore channels between the matrix and the fibre to the outer surface. At the opposite surface, oxygen penetrates through these same channels and reacts with matrix and fibres to form silica. The thickness of the so-formed silica layers increases until the channels are finally closed, thereby preventing further degradation of the carbon interphase. The corresponding reaction scheme is shown in Fig. 12. This macroscopic model developed by Vix *et al.* [37] and Filipuzzi [38] is confirmed in part by our microstructural observations. At low temperature (1223 K), the carbon interphase resists over hundreds of hours, only small CO bubbles forming inside it. At higher temperature (1423 K),

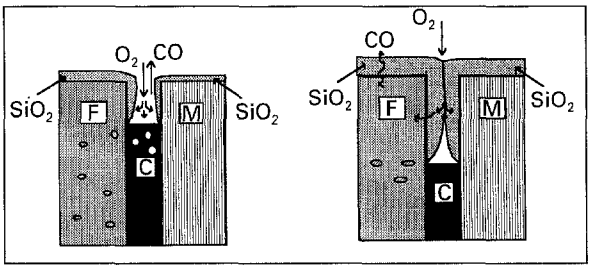

Figure 12 Reaction scheme for the microstructural evolution of the composite in oxidizing atmosphere.

the carbon interphase is progressively substituted by an amorphous silica layer. Small gas bubbles and cracks in the silica layer (visible by TEM) are ascribed to the evacuation of gaseous species through this layer. At still higher temperature (1673 K), the reaction occurs faster and carbon and silica coexist in the same interphase cross section, until complete substitution of carbon by silica. This is in contradiction with the simplified model of Filipuzzi, who assumed that the substitution of the carbon interphase is continuous. Finally, at 1673 K, where the viscosity of amorphous silica is strongly decreased, small pores and cracks are still present in the silica layer.

Similar to the oxidation of pure silicon carbide [32], the oxidation rate of the matrix and probably of the fibre from the oxygen in the pore channels is probably controlled by a mixed mechanism, involving diffusion of oxygen and counterdiffusion of carbon monoxide across the protective silica scale and chemical reaction rate at the interface itself. Matrix oxidation at the surface and next to the pore channels can be described by a simple oxidation reaction (Equation 9).

Our observations indicate the presence of a crystalline silica layer on the composite surface after oxidation, as well as the presence of an amorphous silica layer, which has replaced the carbon interphase. This is in contradiction with observations by Fretty [39], who detected in similar conditions a cristobalite layer around the fibres. However, the amorphous character of the layer is not surprising, since it grew on top of the fibre and therefore easily matched the amorphous structure of the oxycarbide. Crystallization may occur for very long annealing times or in the presence of impurities which may act as nuclei. The oxidation on the fibre side of the channel is more complex, because all three phases which constitute the fibre can be oxidized

$$SiC_{(f)} + 3/2O_2 \Rightarrow SiO_2 \text{ (or } SiO_xC_y) + CO \quad (9)$$

$$C_{(f)} + 1/2O_2 \Rightarrow CO \quad (11)$$

$$zSiO_xC_{y(f)} + 1/2O_2 \Rightarrow zSiO_{x+\delta}C_y(\text{or } SiO_2) \quad (13)$$

(oxygen enrichment of oxycarbide phase)

As can be seen from Equations 9–11 and 13, oxidation of the fibre leads to formation of carbon monoxide and silica. The global reaction, averaged over the heterogeneous microstructure, follows the same reaction scheme as the oxidation of silicon carbide on the

matrix side, but should be accelerated by the presence of easily oxidizable graphite crystals.

Oxygen diffusion can occur from the silica layer into the fibre, yielding enrichment of the oxycarbide phase in silica and partial dissolution of the small graphite and silicon carbide crystallites. Our chemical microanalysis of the fibres confirm such an oxygen diffusion into the fibre. They indicate a global enrichment in oxygen of the fibres during treatment in an oxidizing atmosphere. In addition, high resolution imaging reveals a lower amount of silicon carbide and carbon crystals in the fibre next to the silica interphase, as compared to the bulk fibre.

5. Conclusions

A SiC–C–$SiC(O)_{fibre}$ composite was annealed at temperatures ranging from 1123 to 1673 K, under different oxygen partial pressures and activities of carbon, silica or silicon carbide of one at the outer surface. The annealed materials were investigated by analytical scanning electron microscopy, by transmission electron microscopy with EDX and EELS analysis and by HREM. Reaction modes for the high temperature corrosion of SiC–C–$SiC(O)_{fibre}$ composites were developed on the basis of thermodynamical considerations and in agreement with experimental observations. In all annealing conditions, a reaction front penetrates from the outer surface into the bulk composite.

In reducing atmosphere the matrix remains unmodified; only the fibres lose oxygen, which is evacuated as CO or SiO to the outer surface. Oxygen loss is reflected in the global decrease of the amount of silicon oxycarbide in the fibre. The fibre is porous and made of larger silicon carbide crystals and graphite crystals, which are surrounded by a thin amorphous layer of silicon oxycarbide. Next to the interphase, silicon oxycarbide of the fibre reacts with carbon of the interphase to form silicon carbide and carbon monoxide, leaving a pore channel to the outer surface and a ring of silicon carbide crystals. The pore channel can be filled by further reduction of the fibre and growth of the silicon carbide ring.

In neutral atmosphere the fibre degrades by formation of CO and SiO as gaseous products and therefore becomes very porous upon annealing. The carbon interphase is oxidized by reaction with the surrounding gas, forming large pore channels around the fibres. Next to the fibre interface carbon from the interphase may react with the fibre degradation product, SiO, and form a mixed silica/silicon carbide scale. Fibre and matrix are oxidized by gas diffusion along the pore channels, resulting in the formation of thin silica scales. Since the growth of these scales is slow, the pore channels are not filled, and the composite is not protected against corrosion of the bulk.

In oxidizing atmosphere, all three phases of the composite are oxidized. The carbon interphase is rapidly oxidized, leaving pore channels, which allow penetration of oxygen into the channel and evacuation of carbon monoxide. Oxidation of the fibre and specially of the matrix is less rapid. The oxidation product is amorphous silica growing on top of the fibre and the matrix, into the pore channels and consequently filling them. Then silica forms a protective layer for the bulk composite, against further rapid oxidation of the carbon interphase. The silica layer continues to grow by further consumption of the fibre and evacuation of CO through the silica layer.

Acknowledgements

The authors want to thank J. Deschamps, D. Imhoff and B. Pellissier, Laboratoire de Physique des Matériaux, for their contributions to the experimental part of the work and for helpful discussions. They want to mention that this study was realised in the framework of the GS4C on "thermostructural properties of fibre reinforced composites" and supported by CNES, CNRS, DRET, MRE, Aerospatiale, SEP and SNECMA. Special thanks are due to SEP for providing the materials and collaboration.

References

1. M. LANCIN, J. THIBAULT-DESSEAUX and J. S. BOUR, *J. Microsc. Spectrosc. Electron.* **13** (1988) 503.
2. X. J. NING and P. PIROUZ, *J. Matter. Res. Soc.* **6** (1991) 2234.
3. X. J. NING, P. PIROUZ and S. C. FARMER, *J. Amer. Ceram. Soc.*, **76** (1993) 2033.
4. T. F. COOKE, *ibid.* **74** (1991) 2959.
5. S. YAJIMA, K. OKAMURA, J. HAYASHI and M. OMORI, *ibid.* **59** (1976) 324.
6. S. YAJIMA, Y. HASEGAWA, J. HAYASHI and M. IIMURA, *J. Mater. Sci.* **13** (1978) 2569.
7. Y. HASEGAWA, M. IIMURA and S. YAJIMA, *ibid.* **15** (1980) 720.
8. K. OKAMURA, *Composites* **18** (1987) 107.
9. R. NASLAIN, O. DUGNE, A. GUETTE, J. SEVELY, C. R. BROSSE, J. P. ROCHER and J. COTTERET, *J. Amer. Ceram. Soc.* **74** (1991) 2482.
10. H. C. CAO, E. BISCHOFF, O. SBAIZERO, M. RUHLE and A. G. EVANS, *ibid.* **73** (1990) 1691.
11. X. BOURRAT and C. DROILLARD, Actes de la seconde journée scientifique sur les composites thermostructuraux (1993) 13.
12. D. IMHOFF, M. BACKHAUS-RICOULT and N. MOZDZIERZ, in press.
13. Y. SASAKI, Y. NISHINA, M. SATO and K. OKAMURA, *J. Mater. Sci.* **22** (1987) 443.
14. M. GUIGON, *Rev. Phys Appl.* **23** (1988) 229.
15. C. LAFFON, A. M. FLANK, P. LAGARDE, M. LARIDJANI, R. HAGEGE, P. ORLY, J. COTTEREY, J. DIXMIER, J. L. MIQUEL, H. HOMMEL and A. P. LEGRAND, *J. Mater. Sci.* **24** (1989) 1503.
16. L. PORTE and A. SARTRE, *ibid.* **24** (1989) 271.
17. P. SCHRECK, C. VIX-GUTERL, P. EHRBURGER and J. LAHAYE, *ibid.* **27** (1992) 4237.
18. S. M. BLEAY, A. R. CHAPMAN, G. LOVE and V. D. SCOTT, *ibid.* **27** (1992) 5389.
19. P. LE COUSTUMER, M. MONTHIOUX and A. OBERLIN, *J. Eur. Ceram. Soc.* **11** (1993) 95.
20. M. MONTHIOUX, Rapport GC4C (1991).
21. N. MOZDZIERZ and M. BACKHAUS-RICOULT, Rapport GS4C (1991).
22. C. LABRUGERE, A. GUETTE and R. NASLAIN, Rapport GS4C (1991).
23. J. VINCENS, M. H. ROUILLON, P. FOURVEL, F. ABBE, M. GOMINA and J. L. CHERMANT, *Microsc. Microanal. Microstruct.* **2** (1991) 75.
24. PP. GREIL, *J. Eur. Ceam. Soc.* **6** (1990) 53.
25. K. L. LUTHRA, *J. Amer. Ceram. Soc.* **69** (1986) C-231.

26. T. MAH, N. L. LECHT, D. E. Mc CULLUM, J. R. HOENIGMAN, H. M. KIM, A. P. KATZ and H. A. LIPSITT, *J. Mater. Sci.* **19** (1984) 1191.
27. G. S. BIBBO, P. M. BENSON and C. G. PANTANO, *ibid.* **26** (1991) 5075.
28. S. M. JOHNSON, R. D. BRITTAIN, R. H. LAMOREAUX and D. J. ROWCLIFFE, *J. Amer. Ceram. Soc.* **71** (1988) C-132.
29. M. H. JASKOWIAK and J. A. DICARLO, *ibid.* **72** (1989) 192.
30. H. ZHANG and C. G. PANTANO, *ibid.* **73** (1990) 958.
31. G. D. SORARU, V. M. SGLAVO, G. D'ANDREA and F. BABONNEAU, *Third Euro. Ceramics* **2** (1993) 1157.
32. K. L. LUTHRA, *J. Amer. Ceram. Soc.* **74** (1991) 1095.
33. C. LABRUGERE, A. GUETTE and R. NASLAIN, Rapport GS4C (1992).
34. C. LABRUGERE, A. GUETTE and R. NASLAIN, *Rev. Composites et Matér. Avançés* **3** (1993) 91.
35. N. MOZDZIERZ and M. BACKHAUS-RICOULT, *ibid.* **3** (1993) 49.
36. N. MOZDZIERZ and M. BACKHAUS-RICOULT, Rapport GS4C (1992).
37. C. VIX, Thesis, Université de Haute Alsace, 1991.
38. L. FILIPUZZI, Thesis Université Bordeaux I, 1991.
39. N. FRETTY, R. MOLINS and M. BOUSSUGE, *J. Mater. Sci.* **27** (1992) 5084.

Received 21 December 1993
and accepted 25 November 1994